Tuning Catalytic Reactivity via Wetting Control Through Oxygen Vacancies: Ru Clusters on Anatase TiO_2 and CeO_2 Supports

Linxiao Chen,[1, 2, 9]* Carrington G. Moore,[2, 3] Charles E. Umhey,[3] Jorge E. Perez-Aguilar,[4] Jiyun Hong,[4] Adam S. Hoffman,[4] Ryan M. Thorpe,[5] Julia B. Moreira,[2] Libor Kovarik,[2] Simon R. Bare,[4] Simone Raugei,[2]* Jean-Sabin McEwen,[2, 3, 6, 7, 8] * and Janos Szanyi[2]*

[1] Department of Chemical, Biological, and Corrosion Engineering, The University of Akron, Akron OH 44304, USA

[2] Institute for Integrated Catalysis, Pacific Northwest National Laboratory, Richland WA 99352, USA

[3] Voiland School of Chemical Engineering and Bioengineering, Washington State University, Pullman WA 99164, USA

[4] Stanford Synchrotron Radiation Lightsource, SLAC National Accelerator Laboratory, Menlo Park CA 94025, USA

[5] Institute for Functional Materials and Devices, Lehigh University, Bethlehem PA 18015, USA

[6] Department of Physics and Astronomy, Washington State University, Pullman WA, 99164, USA

[7] Department of Chemistry, Washington State University, Pullman WA, 99164, USA

[8] Department of Biological Systems Engineering, Washington State University, Pullman WA, 99164, United States

[9] Department of Chemistry, University of North Texas, Denton TX, 76201, United States

*Corresponding authors: linxiao.chen@unt.edu; simone.raugei@pnnl.gov; js.mcewen@wsu.edu; janos.szanyi@pnnl.gov

Abstract

The shape of supported metal particles regulates their catalytic reactivity and is determined by the degree of wetting between the metal particle and the support surface. Flattened particles that wet support surfaces were reported in various catalytic systems, particularly in the sub-nanometer size regime. Such consequential metal-support wetting phenomena are poorly understood, and methods to study them on powder catalysts under realistic conditions are lacking. Here, we investigate the size-dependent wetting behaviors of Ru particles on two reducible-oxide supports, anatase TiO_2 (TiO_2-A) and CeO_2, under reducing catalytic conditions. X-ray absorption spectroscopy (XAS), low-energy ion scattering (LEIS), and density functional theory (DFT) are combined to determine the shape of Ru particles. Ru particles remain three-dimensional without wetting the TiO_2-A support within the coverage range studied (0.06 ~ 0.98 Ru nm^{-2}). In contrast, at low coverages (< 0.25 Ru nm^{-2}), Ru wets the CeO_2 support to form flat, disordered structures. The higher wettability of CeO_2 than TiO_2-A is attributed to oxygen vacancies in the near-surface region. The shape difference between small Ru particles or clusters on the two supports leads to drastically contrasting catalytic reactivities in polyolefin hydrogenolysis, despite similar diameters. This work highlights the implications of metal-support wetting, or cluster shape, on catalytic behaviors of small metal clusters, while establishing the foundation for future systematic studies of such a phenomenon in realistic systems, by delivering a multi-technique methodology and revealing governing fundamental principles.

Introduction

The most common types of heterogeneous catalysts are supported metal catalysts, which have active metal particles (herein referring to sufficiently large particles to exhibit well-defined structures and regular metal-atom packing) or clusters (herein referring to sub-nanometer clusters with irregular structure) dispersed on a supporting matrix.[1] The rate and selectivity of structure-sensitive reactions are influenced by the size and shape of metal particles/clusters, depending on the type of exposed facets and sites (terrace, edge, corner, etc.).[2] For unsupported particles, Wulff construction predicts their shapes based on surface energies.[3] Conversely, the shapes of supported particles/clusters are influenced by their interactions with the support and the energy at the metal-support interface (MSI).[4] The shape of a supported metal particle/cluster can be viewed as its degree of "wetting", or the contact angle with the support surface (Scheme 1). This can be described by the Young-Laplace equation

$$\cos\theta = \frac{\gamma_S - \gamma_{MSI}}{\gamma_M}, \qquad \text{(Eq. 1)}$$

where θ is the contact angle between the metal and the support, γ_S and γ_M are the surface energies of the support and the metal, respectively, and γ_{MSI} represents the excess energy of the metal-support interface relative to the bulk.[5] Thus, a supported metal particle/cluster may adopt a flattened shape ("wet" the support; $\theta << 90°$), rather than the three-dimensional form expected in the non-supported scenario, assuming sufficiently strong metal-support interactions (low γ_{MSI}), high γ_S, and/or low γ_M. Flattened particles/clusters have been serendipitously reported in various catalytic systems, often showing distinct reactivities compared to three-dimensional ones.[4, 6-34]

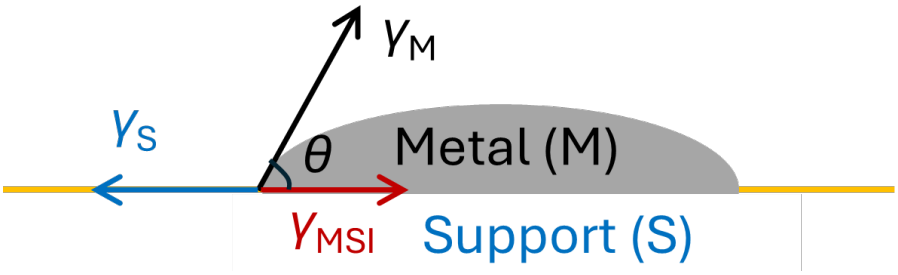

Scheme 1. Wetting of a support surface by a metal particle determines the particle shape.

Despite the broad, significant implications in catalysis, studies to understand the general principles governing metal-support wetting are rare. The groundbreaking work by Campbell et al., developed a framework to predict the wetting in ultra-high-vacuum (UHV) single-crystal systems.[4, 22-26] The approach is based on calorimetry measurements of the adhesion energy (E_{adh}) at the metal-support interface, defined as $E_{adh} = \gamma_M + \gamma_S - \gamma_{MSI}$. E_{adh} describes the wetting via Eq. 1 re-arranged into the Young-Dupre equation: $\cos\theta = E_{adh} / \gamma_M - 1$.[5] This framework was validated by obtaining θ from modeling low-energy ion scattering (LEIS) data. Unfortunately, compared to ideal model systems (single crystals in UHV), powder catalysts exhibit complex structural heterogeneity and dynamics under realistic catalytic conditions,[35-38] making it impossible to measure E_{adh} directly. Meanwhile, metal-support wetting is more prevalent with sub-nanometer metal clusters, which often demonstrate irregular structures with unique bonding and/or electronic interactions with support surfaces[7-16, 32-34] These properties frequently impart desirable catalytic characteristics distinct from larger particles, but complicate the interpretation of support-wetting behaviors by challenging 1) models based on the surface energy and support interaction of well-defined particles; and 2) structural characterization for shape identification.

We previously reported that under the reducing conditions of catalytic polyolefin (PO) hydrogenolysis, when Ru on CeO_2 are present as clusters of approximately < 1 nm diameter, their

structural characteristics abruptly resemble those of flat rafts.[8] The inferred support wetting by Ru clusters coincides with the emergence of desired reactivity in this crucial reaction for chemical plastic recycling.[39-42] This work aims to understand the size-dependent metal-support wetting behavior by systematically examining and comparing Ru particles/clusters of various sizes on anatase TiO_2 (TiO_2-A) and CeO_2. By combining X-ray absorption spectroscopy (XAS), low-energy ion scattering (LEIS), and density functional theory (DFT), we demonstrate that small Ru particles retain three-dimensional structures on TiO_2-A without wetting it. Consequently, they do not display the unique catalytic reactivities of flat Ru clusters on CeO_2, whose structure was further clarified by this study. The lower wettability of TiO_2-A compared to CeO_2 is attributed to the absence of oxygen vacancies (O_v) in the near-surface region. These results illuminate the fundamental principles that govern metal-support wetting, establishing a novel general multi-technique approach to investigate such behaviors in realistic catalytic systems.

Results

Wetting behaviors of small Ru clusters on reducible supports determine catalytic reactivity

A series of Ru/TiO_2-A powder catalysts (surface area ≈ 180 m^2/g) with the Ru surface coverage between 0.03 and 0.98 nm^{-2} (0.10 ~ 3.1 Ru wt%, Table S1) were synthesized by wet impregnation, and reduced with H_2 at 260 °C. The dependence of the Ru structure on its coverage on TiO_2-A was first examined using *in-situ* Ru K-edge XAS under the reduction condition. Figure 1a shows that in the extended X-ray absorption fine structure (EXAFS), as the Ru coverage increases, scattering intensity from the directly bonded Ru neighbors (i.e., nearest neighbors, which we denote as the Ru−Ru_1 path) is enhanced, suggesting an increasing size of Ru particles.[43]

The best fit model for the EXAFS (Table S2) shows an increase of N(Ru−Ru$_1$) from 6 ± 1 at 0.06 Ru nm^{-2} to 11 ± 1 at 0.98 Ru nm^{-2} (Figure 1c, black), corresponding with ~20 and ~3100 Ru atoms per particle (purple).[43] The Ru particle size on 0.06 Ru/TiO$_2$-A (all samples below denoted as "*x* Ru/MO$_2$", with *x* being Ru coverage in nm^{-2}) derived from the EXAFS agrees well with that acquired from scanning transmission electron microscopy (STEM, d = 1.1 ± 0.3 nm, Figure S6c-f). In the X-ray absorption near-edge spectrum (XANES, Figure 1b), the white-line intensity of Ru/TiO$_2$-A starts higher than that of bulk Ru metal (brown) at 0.06 Ru nm^{-2} (blue). It decreases slightly as the Ru coverage increases, with the overall characteristics approaching those of Ru foil. This is expected since increasing particle size makes Ru atoms, on average, more metallic.

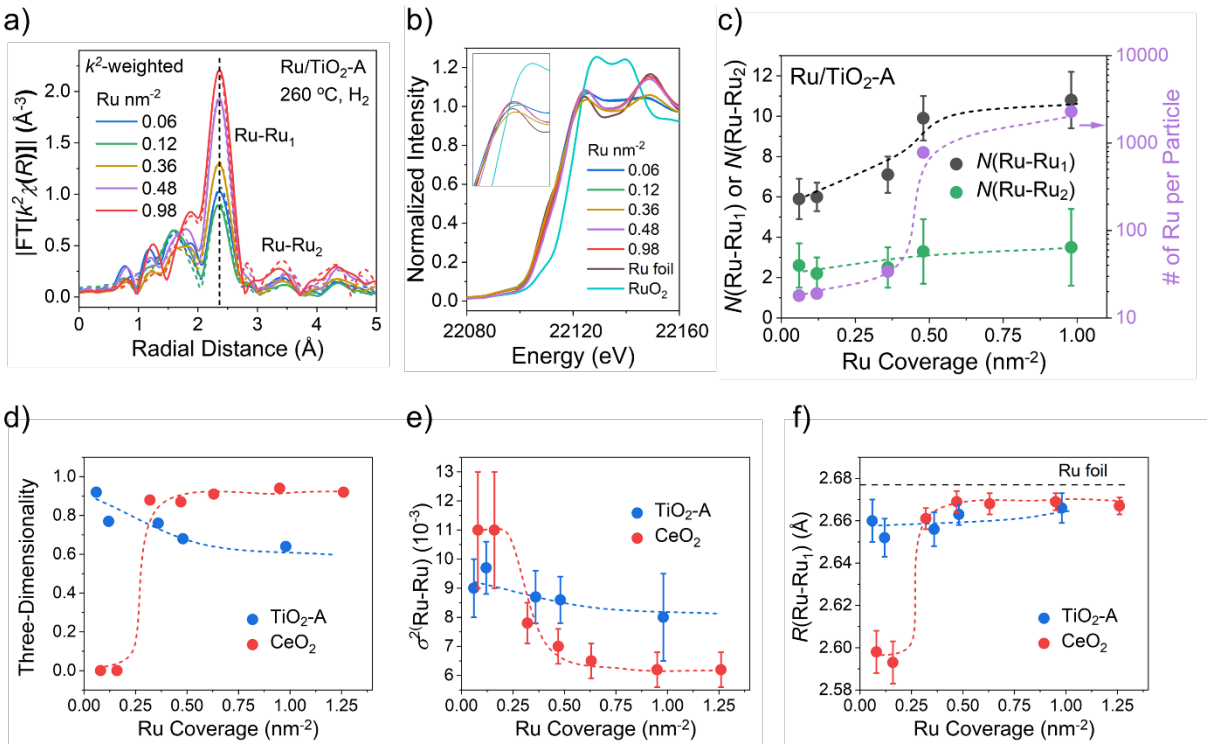

Figure 1. XAS analysis of Ru/TiO$_2$-A with various Ru coverages, compared to Ru/CeO$_2$. a. *R*-space magnitude of k^2-weighted EXAFS, with the best fit models for data between 1 and 4.8 Å shown as the dashed curves. The fitting parameters are shown in Table S2; the *k*-space and *R*-space imaginary parts with fittings are shown only in Figure S5a-b. **b.** Normalized XANES region, with Ru foil and RuO$_2$ spectra shown in brown and cyan, respectively. The inset shows a zoomed-in view of the white-line region. **c.** N(Ru−Ru$_1$), N(Ru−Ru$_2$) values (coordination numbers of the first

and second nearest neighbors, respectively) from the best fits, and the average number of Ru atoms per particle calculated from N(Ru−Ru_1) following an established method.[43] The average particle diameter and dispersion are reported in Table S1. **d** – **f**. Variations in the three-dimensionality, σ^2(Ru−Ru), and R(Ru−Ru_1), respectively, with Ru coverage. Ru/TiO_2-A data are shown in blue, and Ru/CeO_2 data, reported previously,[8] were re-fit using the same model with the Ru/TiO_2-A and plotted in red. XAS data were collected *in-situ* at 260 °C, under 20 bar H_2 for Ru/TiO_2-A and 1 bar H_2 for Ru/CeO_2. All samples were pre-reduced at 260 °C under 30 bar H_2 for > 3 h. Results using an alternative fit model deploying the Debye Model to calculate σ^2 of all Ru−Ru scattering paths are shown in Table S2-Alt and Figure S5c.

In fcc/hcp metals, the second-nearest neighbors of an atom exclusively exist in the packing layers above and below it (three in each, totaling six). We denote Ru−Ru_2 as the scattering path from the second nearest neighbor. Therefore, the ratio between the actual N(Ru−Ru_2) and the predicted N(Ru−Ru_2) from N(Ru−Ru_1), assuming a hemispherical particle shape, can be used to gauge the "three-dimensionality" of Ru particles (see Note S1 in the Supporting Information). Values of 0 and 1 represent perfectly flat (single-layer, $\theta = 0°$) and perfectly three-dimensional structures ($\theta = 90°$), respectively. Figure 1a shows that for Ru/TiO_2-A, the scattering intensity from the Ru−Ru_2 path visually does not exhibit a strong response to Ru coverage, with N(Ru−Ru_2) in the best fits increasing only from 2.6 ± 1.1 at 0.06 Ru nm^{-2} to 3.5 ± 1.9 at 0.98 Ru nm^{-2} (Figure 1c, green; Table S2). Consequently, the three-dimensionality decreases slightly as the Ru coverage increases (shown in blue in Figure 1d), from 0.92 (0.06 Ru nm^{-2}) to 0.63 (0.98 Ru nm^{-2}). These values indicate that on TiO_2-A, small Ru particles maintain and even become more three-dimensional than the larger ones. This contrasts sharply with the trend observed on CeO_2 in this Ru coverage range (Figure 1e-f, red, raw EXAFS data reported previously),[8] where Ru−Ru_2 scattering abruptly vanishes, indicating that Ru clusters become flat and completely wet the CeO_2 surface at < 0.25 Ru nm^{-2} (d = 0.8 ± 0.2 nm in STEM).

Models for Ru particles/clusters (Figure S5d) that appear at $d \approx 1.0$ nm in STEM predict N(Ru−Ru_1) = 3.9 and 6.5 with a flat and a three-dimensional shape, respectively, aligning

reasonably with values from the best EXAFS fits of Ru/CeO_2 and Ru/TiO_2-A at this size (3.3 ± 0.7 and 6 ± 1, Table S2), supporting the concluded shape. Furthermore, the flattening of Ru/CeO_2 at < 0.25 nm^{-2} is accompanied by 1) a sharp increase in the σ^2 disorder factor of Ru−Ru scattering paths (Figure 1e, red), σ^2(Ru−Ru), or a sharp decrease in the Debye Temperature, Θ_D, in the alternative fit model using the Debye Model to calculate σ^2(Ru−Ru) (Figure S5c, Table S2-Alt), both of which indicate a higher level of structural disorder; 2) the abrupt shortening of direct Ru−Ru bonds, R(Ru−Ru_1) (Figure 1f).[8] In contrast, none of these parameters change significantly when the Ru coverage on TiO_2-A decreases to 0.06 nm^{-2} (blue in Figures 1e-f and S5c), further supporting that Ru does not flatten to wet TiO_2-A. In X-ray photoemission spectroscopy ((XPS), collected after re-reduction with no air exposure), 0.06 Ru/TiO_2-A exhibits a lower Ru $3d_{5/2}$ binding energy (Figure S6a, 279.7 eV, close to metallic[44]) than 0.13 Ru/CeO_2 (280.6 eV).[8] Since Ru particles/clusters on the two surfaces have a similar top-projection area (d ~1 nm) in STEM, such observation supports that a smaller fraction of Ru atoms on TiO_2-A are in contact with the oxide-support surface, i.e., Ru structures are more three-dimensional. XPS also shows that the H_2-reduction creates minimal (2.5%) Ti(III) in the near-surface region of Ru/TiO_2-A (Figure S6b), in comparison to 48% Ce(III) in that of Ru/CeO_2 (mean escape depth ≈ 1.1 nm for Ti 2p and Ce 3d photoelectrons[45]).[8] This is consistent with the consensus that TiO_2-A favors bulk O_v,[46-48] while CeO_2 favors near-surface ones.[49, 50]

LEIS further examined the different wetting behaviors of Ru on the two reducible-oxide supports. As a technique that is only sensitive to the topmost surface layer,[51-54] LEIS is less commonly used in powder than single-crystal studies due to surface adsorbates and curvatures.[55] An analytical procedure was developed to minimize such artifacts (details in Note S2 and Table S3 in the Supporting Information). Each sample was re-reduced before the measurement, with no

air exposure. Figure 2a shows that among all Ru/TiO_2-A, the Ru coverage in the first surface layer, calculated from the area of scattering peak from Ru and Ti atoms (see Figure S7a for raw spectra), is proportional to the total Ru coverage, suggesting that as one increases the Ru coverage,[51-54] the cross section of Ru particles grows, but the average height remains similar. In this plot, a slope of 1 in the linear fit going through the origin (marked by the grey dotted line) would indicate Ru structures with a 1-layer height (first-layer Ru = total Ru). The slope on TiO_2-A is ~0.25, corresponding with 4-layer average particle height, suggesting that Ru particles do not completely wet the support. The average particle height was calculated separately for each sample, fluctuating around 4.5 layers (Figure 2c). The relatively constant Ru particle height of ~4 layers aligns with the EXAFS results, which indicate that the particles become more three-dimensional when the size decreases (Figure 1d). The sample with the smallest particles, 0.06 Ru/TiO_2-A, shows $d_{Ru} \approx 1.1$ nm in STEM and three-dimensionality of 0.92, corresponding to particle heights of 3 ~ 4 layers, in reasonable agreement with LEIS. In contrast, among Ru/CeO_2 samples, at < 0.25 Ru nm^{-2}, the first-layer Ru coverage accounts for the total Ru coverage (Figure 2b, see Figure S7b for raw spectra), and the average cluster height is close to 1 layer (Figure 2d), confirming the EXAFS-based conclusion of flat Ru clusters. At > 0.25 Ru nm^{-2}, the average particle height monotonically increases with Ru coverage (Figure 2d), with the first-layer Ru coverage not being proportional to the total Ru coverage (Figure 2b). These observations suggest the formation of three-dimensional particles that expand in all directions, aligning with the EXAFS characteristics.

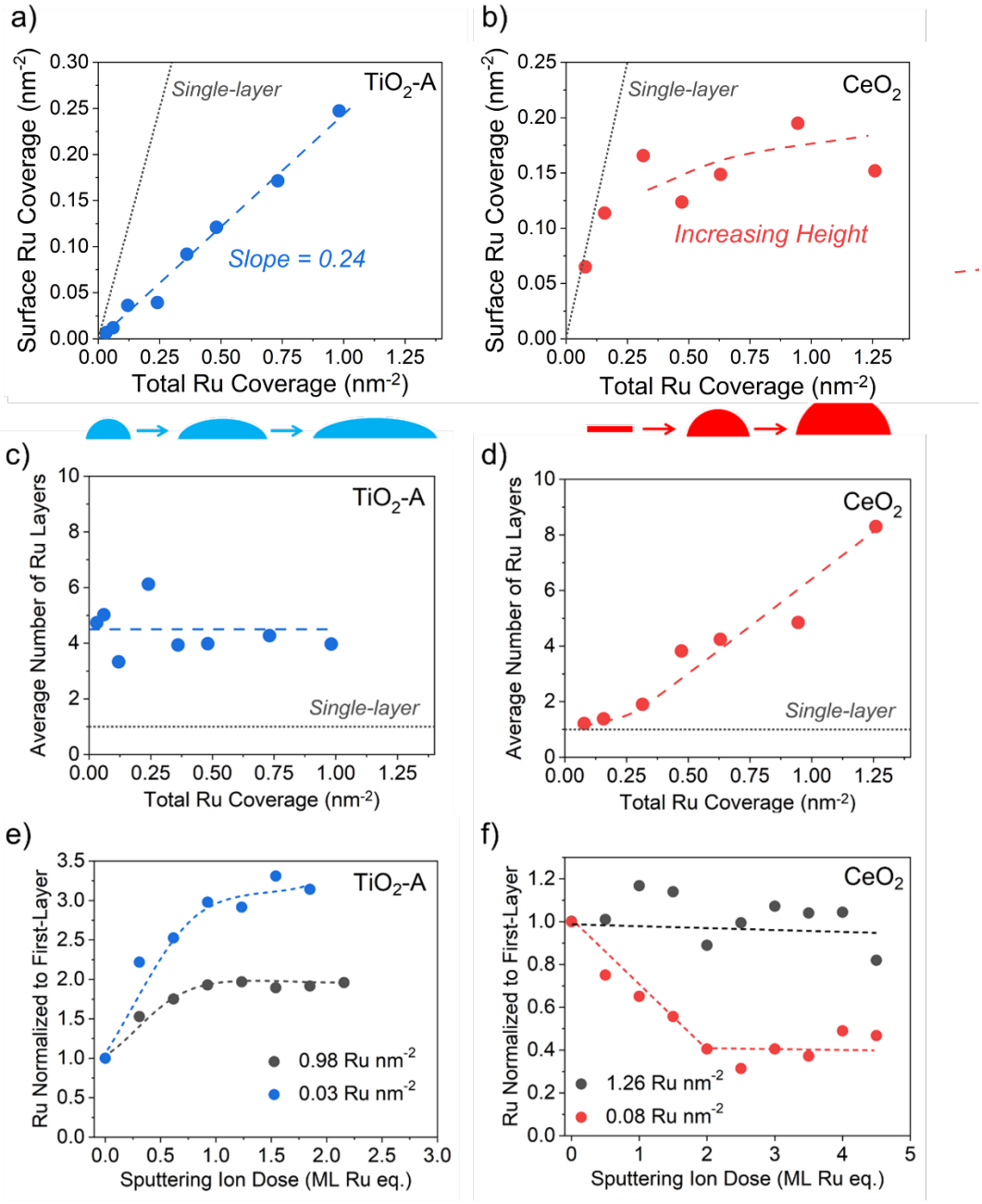

Figure 2. LEIS analysis of Ru/TiO_2-A and Ru/CeO_2. a – b. Ru coverage in the first surface layer plotted against total Ru coverage. **c – d.** Average number of Ru layers (i.e., "particle/cluster height") as a function of total Ru coverage. Procedures to calculate these values are described in Note S2 and Table S3 in the Supporting Information. **e – f.** Ru count as a function of Ar^+ sputtering dose (1 ML Ru eq. = 1.62×10^{15} cm^{-2}), normalized to the count before sputtering (i.e., depth profile of Ru atoms). Only samples with the lowest and highest Ru coverages on each support are shown for clarity. Complete data are available in Figure S7c-d. Prior to LEIS measurements, each sample was re-reduced in a side chamber with ~15 mbar H_2 at 260 °C, and transferred to the measurement chamber with no air exposure. All samples were pre-reduced at 260 °C under 30 bar H_2 for at least 3 h.

To acquire the atomic depth profile, LEIS was repeatedly measured on each sample after several Ar^+ sputtering steps that removed surface atoms. Figure 2e and S7c show that all Ru/TiO_2-A samples exhibit qualitatively similar depth profiles, with increasing Ru counts until sputtering Ar^+ dose reaches ~3×10^{15} cm^{-2} (equivalent to approximately 2 ML of metallic Ru; the sputtering yield of Ru with 0.5 keV Ar^+ is close to 1.0).[56] The initial increase in counts was also observed on the samples for Ti atoms (Figure S7e), and the bulk Ru reference (Figure S7f). This was attributed to removing adventitious surface adsorbates (e.g., carboxylates), and TiO_2 is known for the strong tendency to form such adsorbate layers.[7, 57, 58] On Ru/TiO_2-A, decreases in Ru counts after sputtering were not observed because, as the geometric model (Scheme S1a) shows, removing 1 ML Ru atoms from a hemispherical particle with the sputtering ion beam reduces counts from the primary ion beam by ~1 atom per particle cross section. This translates into ~25% and ~5% count loss for d_{Ru} = 1 and 5 nm, respectively, which are easily offset by the strong count-enhancement effects from adsorbate removal (1.7- to 3-fold in Figure S7c). Meanwhile, Figures 2f and S7d show that Ru/CeO_2 samples exhibit drastically different Ru depth profiles in the flat (< 0.25 nm^{-2}) and three-dimensional (> 0.25 nm^{-2}) regimes. Samples with > 0.25 Ru nm^{-2} show minimal changes or slight increases in Ru counts after Ar^+ sputtering doses equivalent to ~4 ML Ru, which follows the same rationalization as Ru/TiO_2-A samples with three-dimensional particles, and CeO_2 has much less adventitious adsorbates than TiO_2-A (Figure S7e-f). In contrast, samples with < 0.25 Ru nm^{-2} exhibit a fast, steady decrease in Ru counts during the first 2 ML sputtering, before stabilizing at ~40% of the first-layer values. Such behavior suggests that most Ru on < 0.25 nm^{-2} Ru/CeO_2 have flat structures that can be removed entirely within 2-ML sputtering (Scheme S1b; see Note S2 in the Supporting Information for detailed discussions). These results align well with the EXAFS characteristics (Figure 1) and surface coverage analysis from LEIS (Figure 2b and 2d).

In our previous study of polyolefin (PO) hydrogenolysis on Ru/CeO_2, in the range that Ru wets CeO_2 (< 0.25 nm^{-2}), a drastically higher rate and lower selectivity toward the undesired product CH_4 (S_{CH4}) were observed.[8] As the EXAFS and LEIS data agree that Ru particles remain three-dimensional and rigid on TiO_2-A in the entire coverage range, we expected their reactivity in the reaction to follow trends on regular three-dimensional particles, rather than the one observed on Ru/CeO_2. Figure 3a shows that at 260 °C under 30 bar H_2 (similar conditions with the reduction conditions of the samples), the intrinsic conversion rate of polypropylene (PP, in $g_{PP} \cdot g_{surface\ Ru}^{-1} \cdot h^{-1}$) on Ru/TiO_2-A decreases monotonously as one decreases the Ru coverage (blue), in sharp contrast to the abrupt U-turn on Ru/CeO_2 at < 0.25 nm^{-2} (red). The negative rate dependence on particle size was widely reported in alkane hydrogenolysis and attributed to an ensemble-size requirement for the dehydrogenative adsorption of C−C bonds on particle terraces prior to C−C bond cleavage.[59-66] The fact that all Ru/TiO_2-A samples with regular Ru particle structures follow such an established trend is expected. The flat Ru structures on CeO_2 avoid this rate dependence, likely by providing terrace-like Ru ensembles despite their small size.

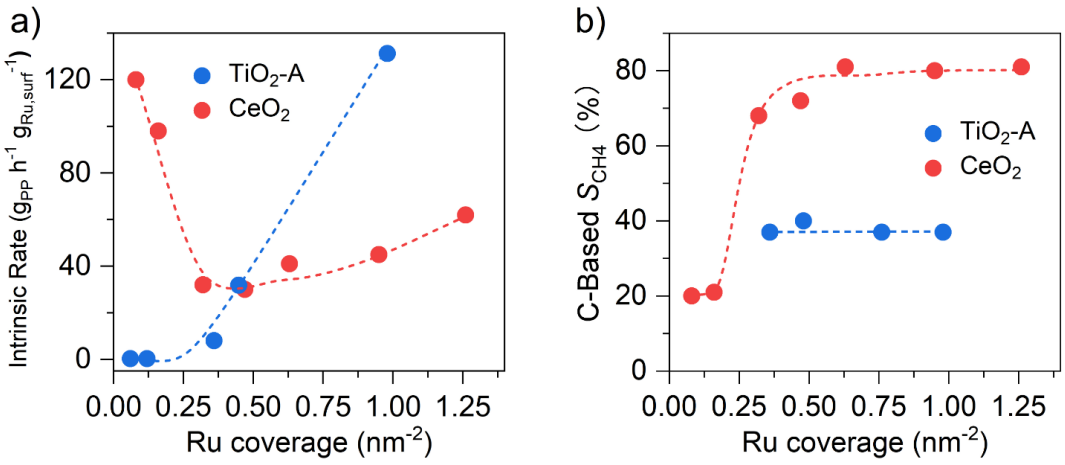

Figure 3. PP hydrogenolysis results on Ru/TiO_2-A (blue) and Ru/CeO_2 (red, replotted from Ref 8). a. intrinsic rate as a function of Ru coverages; **b.** carbon-based selectivity toward CH_4 (S_{CH4}) as a function of Ru coverages (full product distribution in Figure S8). Reaction conditions: 260 °C, 30 bar H_2, m_{alkane} = 1 g, m_{Ru} = 0.5 mg, ~ 18 h, X(PP) < 50% to avoid secondary reactions.[39]

Similarly, Figure 3b shows constant S_{CH4} across all Ru/TiO_2-A with measurable rates (blue), without the abrupt decrease seen on Ru/CeO_2 when the metal-support wetting occurs (red). PO hydrogenolysis under the testing conditions is known to operate in *H-deficient regimes, and the surface coverage of *H is the key negative descriptor for S_{CH4}.[8, 39, 41, 67] The large σ^2(Ru−Ru) or high Θ_D of flat Ru clusters on CeO_2 suggest disordered structures, i.e., weak Ru-Ru interactions. This should enhance the electron-sharing between Ru and *H, leading to reported strong *H adsorption, and thus high *H coverage on them.[8] The rate enhancement can also be explained by the high *H coverage. Since the three-dimensional small Ru particles on TiO_2-A maintain regular structural order, with σ^2 typical for particles of nm-sizes at the measurement temperature and Θ_D typical for supported particles, the lack of drastic changes in S_{CH4} is also expected. The fact that similarly sized Ru particles/clusters ($d \approx 1$ nm) on the two reducible supports display entirely different reactivities emphasizes the significant role of particle/cluster shape, i.e., metal-support wetting in catalysis.

Computational prediction of the size-dependent wetting of reducible oxides by Ru clusters

The wettability of TiO_2-A and CeO_2 surfaces by Ru was studied within a DFT-based model by adsorbing flat (F) or multi-layer (M) Ru structures on them. Three Ru sizes, 13-atom (Ru_{13}), 7-atom (Ru_7), and 4-atom (Ru_4) were tested for each case. Based on experimental XPS results,[8] 0.25 ML of O_v was added to the CeO_2 surface and distributed within the subsurface according to the literature.[49] Ru structures were also examined on a pristine (O_v-free) CeO_2 surface to assess the impact of O_v on the Ru structure and surface wettability (Figure S14). The initial arrangement of the flat Ru clusters had atoms evenly on the surface (see Figure S10 for TiO_2 and Figure S13 for CeO_2), whereas the multi-layer structures featured stacked layers of atoms. Adsorption energies

were calculated relative to the bulk Ru metal (see Table S5 for values with spherical Ru_{13} reference state, Figure S1). The most favorable structures for the three Ru cluster sizes obtained from geometry optimizations are shown in Figure 4 along with the corresponding adsorption energies (where smaller adsorption energies are more favorable, Eqn. S1). In all cases involving TiO_2-A, the most favorable adsorption position occurred when the Ru cluster base was situated between two O_{2c} rows or directly above the saw-tooth gap that characterizes the TiO_2-A (101) surface, more effectively illustrated in Figure S10b, d, and f. In the case of CeO_2, the Ru clusters preferentially locate at the center of a triangle formed by three oxygen vacancies (O_v). The 4F structure, however, was an exception, whereby the cluster situated directly above an O_v site is the most favorable.

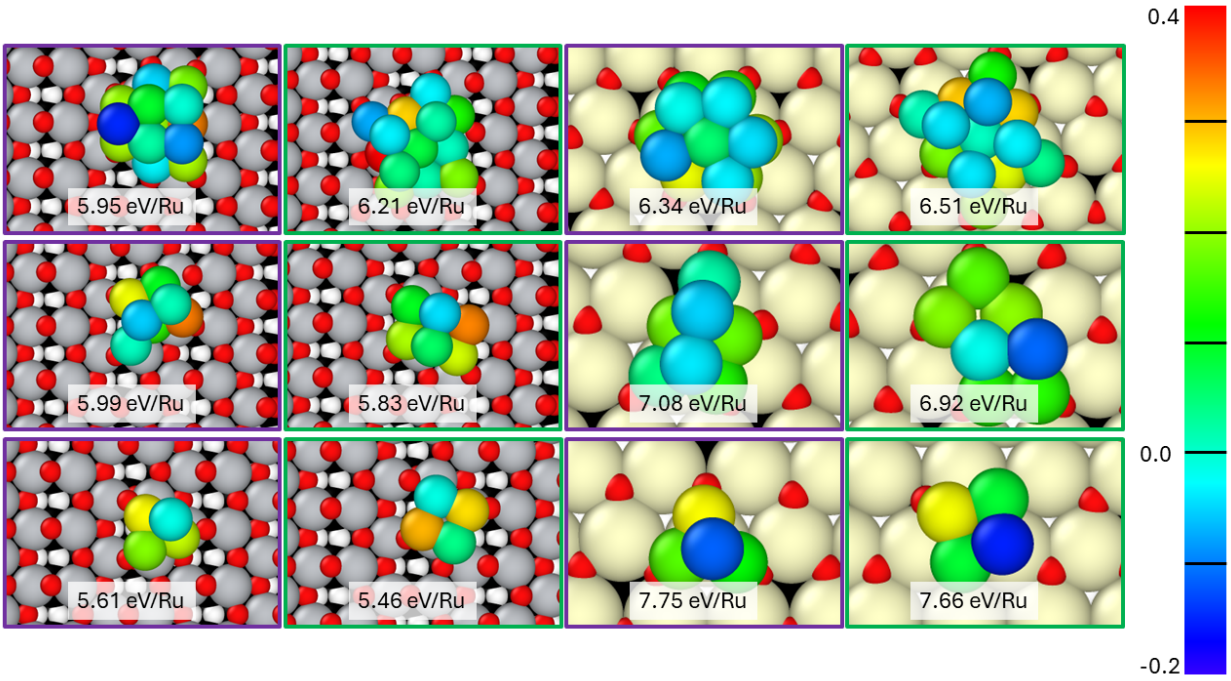

Figure 4. Optimized geometries and adsorption energies for initially flat (green boundary) and multilayer (purple boundary) Ru_{13} (top), Ru_7 (middle), and Ru_4 (bottom) clusters on TiO_2-A (left) and CeO_2 (right). Ru atoms are colored based on the Bader charge population (in fraction of electron charge).

The optimized "F" and "M" structures were compared for each cluster size and support surface. On TiO_2, the 13M structure features a 2-layer stacking of the Ru atoms (Figure 4), arranged such that the base layer, comprising 8 Ru atoms that contact the surface (the metal support interface), is topped by 5 additional Ru atoms. In contrast, during the geometry optimization, the Ru atoms in the 13F structure moved from a single-layer geometry to a puckered structure (Figure 4) with no clear differentiation between the first and second layers. This observation, along with the lower adsorption energy of the 13M structure compared to that of the 13F structure, indicates that the wetting of TiO_2-A by Ru_{13} is not favored. Similar results were obtained for the 7F and 7M clusters. Although the 7F structure has a more favorable adsorption energy than the 7M structure (Figure 4), the initially flat 7F configuration also transforms into a 2-layer structure, similar to the 13F structure. In both final 7F and 7M structures, the base layer consists of 5 atoms, with two atoms layered on top. During geometry optimization, the spontaneous layering of the 7F structure suggests that flat Ru_7 structures are unstable, indicating that Ru_7 does not wet TiO_2-A. Lastly, the 4F structure (Figure 4) is the preferred structure and remains flat throughout the geometry optimization process. The 4M is a spherical structure with three atoms at the base and one on top, which is less favorable than 4F. This indicates that tiny Ru clusters could potentially wet the TiO_2-A surface. In both layered structures of Ru_7 (7M and 7F), the base includes 5 Ru atoms. Additionally, Ru_5 clusters are found to prefer a multi-layer structure over the flat structure by 0.14 eV/Ru (Figure S9). These observations imply that the critical size required for Ru to wet TiO_2-A is less than Ru_5.

To further analyze the "flatness" of the Ru clusters, we examined the height of each Ru atom (*z*-distance above the support surface) from the TiO_2-A surface (Figure 5). The statistical analysis is based on the final configuration reflected in Figure 4 and is in reference to each

individual atom in the clusters analyzed. Therefore, the minimum is in reference to the smallest atom *z*-distance above the surface within the cluster, and the maximum is the largest atom *z*-distance above the cluster, which in the case of stacking is a 2 ML layering. The average height difference between 4F and 4M Ru atoms is 0.2 Å, with the maximum height being noticeably larger (1.2 Å) for the latter due to its well-defined two-layer structure. This maximum height difference is less significant in the cases of Ru_7 (0.56 Å) and Ru_{13} (0.58 Å), as the 7F and 13F structures rearrange into multi-layer configurations (Figures 4, S10). The trend in minimum height varies; the 4M structure exhibits a smaller value than the 4F, while the opposite is true for Ru_{13} and Ru_7. For Ru_4, the 4F structure has all its atoms in the base at nearly the same level. In contrast, the 4M structure has rearranged, with one Ru atom filling the gap created by the saw-tooth, while the other two Ru atoms in the base are positioned at the edge of the saw-tooth near the O_{2c} atoms. The 13M also has the base atoms almost at the same level, leaving the saw-tooth gap empty, whereas 13F is disordered and has some base atoms filling the saw-tooth gap (Figure 4). This results in smaller minimum height values for 13F and 4M than their counterparts. The 7F exhibits this phenomenon, with its base rearranging to fill the saw-tooth gap with a Ru atom, leading to a smaller minimum height than 7M. Such a rearrangement is more favorable than in the 13M and 4F cases.

On the CeO_2 surface (with 0.25 ML O_v), the 13F structure partially layers during geometry optimization, with 4 Ru atoms rising above the plane of the initial flat cluster (Figure 4). However, the average height of these atoms is 0.49 Å lower than the average height of Ru atoms in the second layer of the 13M structure, indicating an incomplete layering process. This can be easily seen in Figure 4. This is similar for the TiO_2-A support, where the 13F structure begins to layer but does not result in distinct layers (Figure 4). Unlike the TiO_2 system, the 7F structure on CeO_2 does not

undergo any layering during geometry optimization. This is evident in the difference between the minimum and maximum heights of Ru atoms: for CeO_2, the 7M structure shows a height variation of 2.07 Å, while the 7F structure shows only 1.11 Å — a difference of 0.96 Å between the two. In contrast, the TiO_2 system exhibits a height difference of 2.43 Å for the 7M structure and 2.32 Å for the 7F structure, resulting in a much smaller change of just 0.11 Å. This indicates that both the 7M and 7F structures in TiO_2 are optimized into a layered configuration, whereas in CeO_2, only the 7M structure is layered, and the 7F structure remains relatively flat. Importantly, the flat 7F structure is energetically more favorable than the 7M structure on CeO_2, in contrast to TiO_2-A, where more compact, layered structures are preferred. This energetic preference for flatness suggests that Ru clusters exhibit higher wettability on CeO_2, whereas on TiO_2-A, only smaller clusters like Ru_4 favor flat configurations. The trend is consistent with experimental data (Figures 1-2). The 4F structure on CeO_2 remains flat during geometry optimization showing a difference between the maximum and the minimum height of 0.89 Å while this difference becomes 2.00 Å for the 4M structure. The 4F structure is energetically more favorable than the 4M structure.

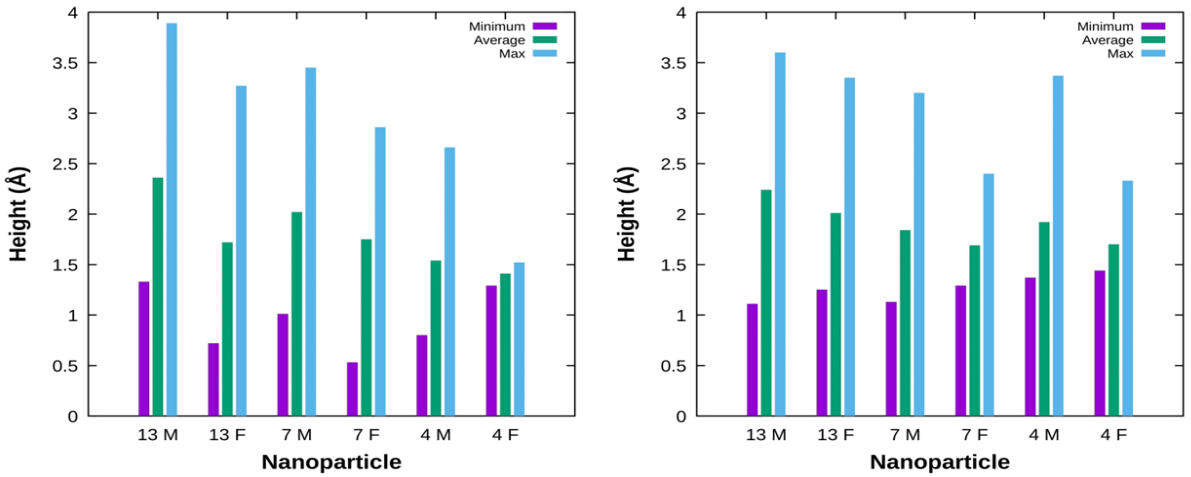

Figure 5. Height information (*z*-distance of Ru nuclei from the surface nuclei) for the three different complexes tested on TiO_2 support (left) and CeO_2 support (right).

Two key points emerge when comparing the pristine CeO_2 surface (Figures S15) and the CeO_2 surface with 0.25 ML O_v. First, Ru clusters adsorb more strongly on the pristine surface with adsorption energies ranging from 5.68 to 6.23 eV/Ru, compared to a range of 6.33 to 7.66 eV/Ru on the CeO_2 surface with O_v when using bulk Ru as the reference. Second, on the pristine CeO_2 surface, Ru clusters do not flatten (see Figure S14 g,h,i,j,k,l). The only initial flat structure that does not spontaneously layer during geometry optimization is the 4F structure, and its adsorption energy is still 0.14 eV/Ru less favorable than the 4M structure. On the surface with O_v, both the 4F and 7F structures have more favorable adsorption energies than their multilayer counterparts and do not spontaneously layer. The comparison suggests that O_v formed under reducing conditions in the near-surface region plays a key role in the wetting of CeO_2 by Ru.

Computational characterization of the electronic and structural properties of supported Ru clusters

We define the positioning and the size of Ru clusters on the TiO_2-A surface as between the two O_{2c} edges of the saw-tooth formation. Further questions remain about why the structure is reordered in this way. Looking at the Bader charge distribution for each Ru atom (Figure 4), we see a trend of positively charged atoms making up most of the metal support interface. The adsorption position of the Ru clusters above the electronegative O_{2c} surface atoms should result in a positive charge for the adsorbed atoms. For multi-layer structures , the most favorable structure has a majority of the interfacial Ru atoms positively charged, consistent with a previous study of Ru clusters on a non-reduced TiO_2 surface.[68] The Ru_4 cluster on both CeO_2 and TiO_2 has the more

favorable 4F structure having one slightly negatively charged Ru atom at the metal support interface. In CeO_2 the 7F structure also has a negatively charged atom at the metal support interface. This can be related to the preference of Ru_4 and Ce-Ru_7 for the flat geometry meaning no 2nd layer positions are available for the negatively charged Ru atoms. Ru_{13} and Ru_7 have the most favorable ground state with a higher number of positive charges than negative ones and with most of the positive charges at the metal support interface. All clusters have a positive overall charge based on the Bader analysis (Table S4). On CeO_2, the Ru clusters show a similar charge distribution, with Ru atoms in the base of multilayer structures being more positively charged than the Ru atom in the second layer. Even in the flat structures, the most negatively charged Ru atoms are found in slightly elevated positions relative to the other atoms in the same layer. Between the pristine CeO_2 surface and the one with 0.25 ML O_v, the latter resulted in a smaller net positive charge for all sizes of clusters analyzed, which is expected because the reduction of CeO_2 increases its electron density. The smallest total net charge observed was the 4F system (0.271 *e*) for CeO_2 and the 4F system (0.597 *e*) for TiO_2-A.

The radial distribution function, $g(R)$, between Ru atoms on the surface, of the most favorable geometry for each cluster shows the nearest Ru neighbor (1NN) interactions between 2-3 Å, while the second-nearest neighbor (2NN) is between 3-4 Å (Figure S11). We see this in TiO_2-A with one peak (2.28 Å) for the 1NN and one peak for the 2NN (3.18 Å) (Figure S11a) for Ru_4. In CeO_2 there are three peaks observed (2.25, 2.95, and 3.35 Å), two for 1NN and one for 2NN (Figure S11d). With the increase in cluster size there is an increase in number of peaks and a broadening of high intensity peaks for both support systems in Ru_7 and Ru_{13}. High intensity peaks for 1NN have an increase of interaction length of ~0.2 Å for TiO_2-A and ~0.1 Å for CeO_2 compared to Ru_4. The 2NN lateral interaction peaks have slight lengthening for TiO_2-A of 0.07 Å, while for

CeO_2 they remain consistent for all three clusters sizes (Figure S11b-f). The 1NN and 2NN distances in these sub-nanometer clusters are generally shorter than those in ordered Ru crystal: $R(\mathrm{Ru{-}Ru_1}) \approx 2.66$ Å and $R(\mathrm{Ru{-}Ru_2}) \approx 3.76$ Å. This reflects the disordered irregular structure of the clusters, echoing with the decrease in $R(\mathrm{Ru{-}Ru_1})$ and increase in σ^2 when Ru wets CeO_2 in the experimental EXAFS results (Figures 1e-f).

We integrated $g(R)$ peaks between 2 and 3 Å and those between 3 and 4 Å to acquire the $N(\mathrm{Ru{-}Ru_1})$ and $N(\mathrm{Ru{-}Ru_2})$ values, respectively. The smallest experimentally available Ru particle on TiO_2-A has 20 ~ 30 Ru atoms (Figure 1c), and the largest one in the theoretical study is Ru_{13}. Although N cannot be compared directly due to size difference, the $N(\mathrm{Ru{-}Ru_2}) / N(\mathrm{Ru{-}Ru_1})$ ratio, which reflects particle/cluster shape (close to "three-dimensionality / 2"), is reasonably close between computation (0.39 for 7F and 0.57 for 13M, Table 1) and experiment (0.43 on 0.06 Ru/TiO_2-A). This result, along with an analysis of the inertia tensor of the clusters[69] (Figure S12), implies that $d \approx 1$ nm Ru clusters have an asymmetric ellipsoid shape on TiO_2-A. In Table 1, the flat structures generated by theory have a lower $N(\mathrm{Ru{-}Ru_2}) / N(\mathrm{Ru{-}Ru_1})$ ratio than the layered ones, as expected. In the $g(R)$ analysis, we defined "NN2" as Ru atoms with 3-4 Å distance. Atoms in the same layer of a defined Ru crystal do not fall in this range, with $R(\mathrm{Ru{-}Ru_1}) \approx 2.66$ Å and $R(\mathrm{Ru{-}Ru_3}) \approx 4.62$ Å. The irregular ordering of the simulated clusters leads to some atoms in the same layer being pushed into this range as distant atoms move closer together and cross the 4 Angstrom threshold needed to qualify as 2NN. This is especially prominent in the 7F structure for CeO_2 where a slight increase in the height of one row of Ru atoms allows neighboring rows to move closer to each other leading to a significant increase in the 2NN/1NN ratio. Similar phenomena can be seen in the 4F clusters as diagonal Ru atoms move closer together and qualify as 2NN. This leads to the non-zero NN2 / NN1 value for the flat structures, and challenges

quantitatively comparing $g(R)$ and the EXAFS analysis. Similar issues are present for all clusters analyzed as the same procedure was used for analysis.

Table 1. Comparison between the computed radial distribution and experimental EXAFS data.

TiO_2-A			CeO_2 (0.25 ML O_v)		
Cluster size	**Geometry**	**NN2 / NN1***	**Cluster size**	**Geometry**	**NN2 / NN1**
Ru_4	Flat	0.32	Ru_4	Flat	0.20
Ru_7	Layered	0.39	Ru_7	Flat	0.67
Ru_{13}	Layered	0.57	Ru_{13}	Layered	0.56
~Ru_{20} (Exp.)	Layered	0.43	~Ru_7 (Exp.)	Flat	0

* NN1 and NN2 are defined as Ru atoms between 2 and 3 Å and those between 3 and 4 Å, respectively. They are similar to the values of $N(Ru{-}Ru_1)$ and $N(Ru{-}Ru_2)$ from the EXAFS fitting.

In summary, DFT supports the experimental conclusion that Ru clusters have a stronger tendency to wet the surface of CeO_2 than the surface of TiO_2-A under reducing conditions. The smaller size of Ru clusters favors wetting, and O_v formed in the near-surface region of CeO_2 is crucial for the wetting.

Summary of the Computational Results

The most favorable adsorption position for the anatase TiO_2 (101) surface is above the saw-tooth ridge inherent to the (101) anatase surface, which is bordered by the O_{2c} surface atoms. This placement remains consistent regardless of the largest or smallest sizes tested (Figure 4). For Ru_4, the preferred configuration is 4F; whereas, for all other complexes tested, the cluster reorganizes and favors a 2-layer structure (13M and 7F). The threshold for the preference for a flat structure is 4 atoms, as the 5-atom structure prefers 2 layers (Figure S9). The most favorable structures display a Bader charge distribution with positively charged Ru atoms at the metal-

support interface and negatively charged Ru atoms in the second layer. Radial distribution information indicates that the closest ratio of NN2 to NN1 to the experimental value is observed in the 7F structure, which will likely adopt an asymmetric top shape (Figure S8). The experimental particles are approximately 10 times larger than the complexes tested here, suggesting that the height and width limits will differ. Therefore, the adsorption position above the saw-tooth at that scale is no longer relevant. As there will be significantly more atoms than in Ru_{13}, the structure is not 2-layered but consists of multiple layers (average 4 layers in Figure 2c). However, the asymmetric top shape and the general configuration of the favored larger base with smaller top layers will likely persist.

The CeO_2 (111) surface has the most favorable adsorption site inside a triangle formed by three oxygen vacancies for all systems except the 4F structure, which forms over a vacancy. Flat cluster shapes were favorable for the Ru_4 and Ru_7 clusters on the surface with vacancies, while no flat clusters were favorable on the pristine CeO_2 surface. As with TiO_2-A, the Bader charge distribution reveals that the bottom layers of the clusters are positively charged, while the top layers are more negatively charged. The radial distribution of clusters on CeO_2 shows very low NN2-to-NN1 ratio in flat Ru_4 that maintains an ellipsoidal shape, aligning with the lack of $N(\text{Ru}-\text{Ru})_2$ in the flat clusters from the experiment.

Discussion

Eq.1 suggests that the metal-support wetting, i.e., the increase in $\cos\theta$, is favored by: 1) higher surface energy of the support (γ_S); 2) lower surface energy of the metal (γ_M); and 3) lower excess energy of the interface (γ_{MSI}), i.e., more stable metal-support interface.[4, 5] From an atomistic

point of view, the flattening of a supported metal particle/cluster gains metal-support interactions at the cost of metal-metal interactions, while stabilizing undercoordinated atoms on the support surface. These governing principles for the wetting are demonstrated in this work. On both TiO_2-A and CeO_2, flat Ru structures are more favorable at smaller sizes. Theory shows a small size limit to favor flat structures (Ru_4 on TiO_2-A; between Ru_7 and Ru_{13} on CeO_2, Figure 4), echoing with the experimental observations that Ru only wets CeO_2 at < 0.25 nm^{-2} (< Ru_{14} from STEM; Ru_7 ~ Ru_{14} from the EXAFS, Figure S5c). This can be understood as supported tiny metal clusters often have irregular metal-metal bonding,[70-72] as suggested by the lower Θ_D than metal foil in the EXAFS fits (Figure S5c). As a cluster grows in size, metal crystals become more ordered, and the increase in metal-metal interaction overcomes the metal-surface interaction, preventing wetting.[30]

The computational case studies described analyzed a bare surface instead of a hydroxylated or hydrogenated surface. A hydrogenated surface is expected to change the particle/cluster shape depending on the hydrogen coverage. When hydrogen is adsorbed at high coverages the particle/cluster begins to change shape and there can be spillover between the H* adsorbed to the metal and the support.[73-75] Other studies have shown that the presence of oxygen vacancies can enhance the migration of H on the surface of CeO_2 by weakening the strength of O-H bonds. Taken together these studies suggest on our surfaces hydroxyl groups should form easier due to the Ru nanoparticles enabling a spillover effect and the H atoms forming the hydroxyl groups should be mobile due to the oxygen vacancies on the CeO_2 surface.[76] On the CeO_2 surface pretreatment with H_2 has been observed to increase Ru nanoparticle dispersion[77] suggesting hydroxyl groups enhance Ru wetting. This could partially be explained by hydroxyl groups forming vacancies in the CeO_2 surface after they desorb to form water, but evidence from in situ DRIFT[77] spectra suggests the hydroxyl groups remaining on the CeO_2 surface can trap and stabilize Ru-O_x complexes enabling

single Ru sites to form. While a detailed description of how these hydroxyl groups influence the shape of Ru nanoparticles is beyond the scope of this work, it is likely such an effect is present and elucidating that effect would be a worthwhile subject of a future study. Computational results show that O_v in the near-surface region, i.e., partial reduction, is required on CeO_2 to be wet by Ru. Two factors could explain this. First, the metal-support interaction comprises two components: local M−O bonding, and the electron transfer at the metal-support "heterojunction" driven by the difference in their work functions (φ). The latter is known to be the dominating driving force for the wetting of MgO thin films by Au particles.[10-16, 78, 79] Literature values of φ_{Ru} (~5.3 eV)[80-82] and $\varphi_{TiO2\text{-}A}$ (~4.4 eV)[83-85] predict electron transfer from TiO_2-A to Ru. Reported φ_{CeO2} values have a wide range between 3.5 and 6.3 eV,[50, 86, 87] but the consensus exists that surface reduction reduces φ_{CeO2} significantly, to < 4 eV.[50, 86, 87] This is intuitive because the reduction injects electrons into CeO_2, elevating its Fermi level. The reduced φ_{CeO2} enhances CeO_2-to-Ru electron transfer, and thus metal-support interaction, reducing γ_{MSI}. Second, O_v created by the reduction destabilize CeO_2 surfaces, i.e., increases γ_S.[50, 88] Both lower γ_{MSI} and higher γ_S would facilitate the wetting (Eq. 1). The effects of near-surface O_v emphasize that the wetting behaviors could vary with reaction conditions.

The two components of the metal-support interaction induce opposite effects on the charge state of Ru. The bonding with electronegative O (3.44 on the Pauling Scale compared to 2.2 of Ru) withdraws electrons from Ru, while the lower φ of TiO_2-A/CeO_2 than Ru drives electron transfer to Ru. Bader analysis (Figure 4) shows that most Ru atoms in the second layer of the clusters carry partial negative charges, while those at the base (at the metal support interface) tend to be positively charged. This is expected because the electron-withdrawing effects from directly bonded O are relatively short-range. At the same time, the electrons transferred due to the

difference in φ should be distributed within the entire cluster. The overall charge of the Ru cluster would hence be determined by the balance between the two. In XANES, < 0.25 Ru nm^{-2} samples on both supports exhibit slightly higher white-line intensity than Ru foil, implying minor depletion of the *p*-band in comparison to bulk Ru metal. This echoes with theory results that on TiO_2-A, Ru atoms have a positive charge, aligning with a previous study that showed that Ru_{10} clusters on TiO_2-A carry 0.5 ~ 1.3 total positive charge.[89] On the pristine CeO_2 surface, Ru clusters also carry slight positive charges (0.07 *e* - 0.78 *e* total, Table S4). The positive charge is reduced by 39% on average on partially reduced CeO_2 (0.03 *e* - 0.55 *e* total), which is expected as the decreased φ_{CeO2} drives more electron transfer to Ru. We previously observed partially negatively charged Pt and Pd flat sub-nanometer clusters on highly reduced oxide supports.[7, 9] Since the level of electron transfer induced by both factors is dependent on the properties of the metal (e.g., electronegativity, work function) and the support (e.g., basicity, work function), predicting the charge state of supported sub-nanometer metal clusters *a priori* is challenging. Density-of-state analysis, coupling *ab initio* calculations with high-energy resolution fluorescence detection (HERFD) XANES, would benefit the detailed understanding of electronic configuration and its effects in catalysis.

Conclusions

This work presents a comparative investigation of the wetting between Ru particles/clusters of varying sizes and two reducible supports, anatase TiO_2 (TiO_2-A) and CeO_2. Flat Ru structures on the support, or metal-support wetting, were identified by: 1) the EXAFS analysis: low $N(Ru{-}Ru_2)$ relative to the predicted value from $N(Ru{-}Ru_1)$ and hemispherical shape; 2) LEIS analysis: similarity between first-layer Ru coverage and total Ru coverage, and sputtering depth profiles; and, 3) theory: more favorable adsorption energy of flat over layered structures, and flat

geometry after optimization. Consistent evidence from these techniques revealed that Ru wets reduced CeO_2 surfaces at < 0.25 Ru nm^{-2} coverage ($d \approx 1$ nm) but remains as three-dimensional rigid particles on TiO_2-A throughout the entire coverage/size range studied herein experimentally. As a result, in polyolefin (PO) hydrogenolysis catalysis, Ru/TiO_2-A exhibit reactivity trends that are well-established among regular particles, without the unique desired activity and selectivity exhibited by flat Ru clusters on CeO_2. Theory and XPS further revealed that O_v formed in the near-surface region of reduced CeO_2, which likely caused its higher wettability than TiO_2-A. This work demonstrates a systematic approach to studying the catalytically consequential metal-support wetting phenomenon on practical catalysts under realistic catalytic conditions, and two key factors governing it: size and oxygen vacancies. This investigation lays the foundation for future efforts to develop a predictive framework for the structure of sub-nanometer metal and metal-oxide clusters supported on reducible oxides. Such a framework could clarify the role of factors such as oxygen vacancies in influencing the wetting behavior of different clusters on these surfaces.[90, 91]

Supporting Information

Detailed description of all methods; supplemental information about all catalysts; supplemental analysis of XAS and LEIS data; EXAFS fitting parameters; XPS and STEM data; notes that detail procedures for EXAFS and LEIS analysis; product distribution from polypropylene hydrogenolysis; second most favorable positions for a multi-layer; Bader charge analysis of ceria surface with oxygen vacancies; Ru_5 clusters on the TiO_2-A surface; moment of inertia analysis; initial structures of Rh nanoparticles on CeO_2 and TiO_2-A surfaces; optimized

geometries, adsorption energies, Mulliken and Bader charge analysis for initially flat and multilayer structures of Ru on ceria.

Acknowledgements

This work was supported by the U.S. Department of Energy, Office of Science, Basic Energy Sciences, Chemical Sciences, Geosciences, and Biosciences Division, Catalysis Science Program, FWP 47319. PNNL is a multiprogram National Laboratory operated for DOE by Battelle. This material is based upon work supported by the National Science Foundation under Grant No. 2430908. L.C. also acknowledges the support from The University of Akron start-up funds. C.U. acknowledges NSF grant CBET-2035280. J.-S.M. was funded by the U.S. Department of Energy, Office of Basic Energy Sciences, Division of Chemical Sciences, Biosciences and Geosciences within the Catalysis Science program, under award number DE-SC0014560. The authors acknowledge X. Shari Li and Mark Engelhard for BET, and XPS measurements. Use of the Stanford Synchrotron Radiation Lightsource, SLAC National Accelerator Laboratory, is supported by the U.S. Department of Energy, Office of Science, Office of Basic Energy Sciences under Contract No. DE-AC02-76SF00515. Co-ACCESS, part of the SUNCAT Center for Interface Science and Catalysis, is supported by the U.S. Department of Energy, Office of Basic Energy Sciences, Chemical Sciences, Geosciences and Biosciences Division 76SF00515. Computational resources were provided by the W. R. Wiley Environmental Molecular Sciences Laboratory (EMSL), a national scientific user facility sponsored by the Department of Energy's Office of Biological and Environmental Research located at Pacific Northwest National Laboratory. This research also used resources of the National Energy Research Scientific Computing Center (NERSC), a Department of Energy Office of Science User Facility using NERSC award BES-

ERCAP0033247. PNNL is a multi-program national laboratory operated for the U.S. DOE by Battelle. LEIS work was performed by the Institute for Functional Materials and Devices at Lehigh University.

References

1. Dai, Y.; Lu, P.; Cao, Z.; Campbell, C. T.; Xia, Y., The Physical Chemistry and Materials Science Behind Sinter-Resistant Catalysts. *Chem. Soc. Rev.* **2018,** *47* (12), 4314-4331.
2. An, K.; Somorjai, G. A., Size and Shape Control of Metal Nanoparticles for Reaction Selectivity in Catalysis. *ChemCatChem* **2012,** *4* (10), 1512-1524.
3. Marks, L. D., Particle Size Effects on Wulff Constructions. *Surf. Sci.* **1985,** *150* (2), 358-366.
4. Zhao, K.; Auerbach, D. J.; Campbell, C. T., Predicting Adhesion Energies of Metal Nanoparticles to Support Surfaces, Which Determines Metal Chemical Potential versus Particle Size and Thus Catalyst Performance. *ACS Catal.* **2024,** *14* (17), 12857-12864.
5. Schrader, M. E., Young-Dupre Revisited. *Langmuir* **1995,** *11* (9), 3585-3589.
6. Gao, S.; Schmidt, L. D., Effect of Oxidation-Reduction Cycling on C_2H_6 Hydrogenolysis: Comparison of Ru, Rh, Ir, Ni, Pt, and Pd on SiO_2. *J. Catal.* **1989,** *115* (2), 356-364.
7. Chen, L.; Allec, S. I.; Nguyen, M.-T.; Kovarik, L.; Hoffman, A. S.; Hong, J.; Meira, D.; Shi, H.; Bare, S. R.; Glezakou, V.-A.; Rousseau, R.; Szanyi, J., Dynamic Evolution of Palladium Single Atoms on Anatase Titania Support Determines the Reverse Water–Gas Shift Activity. *J. Am. Chem. Soc.* **2023,** *145* (19), 10847-10860.
8. Chen, L.; Meyer, L. C.; Kovarik, L.; Meira, D.; Pereira-Hernandez, X. I.; Shi, H.; Khivantsev, K.; Gutiérrez, O. Y.; Szanyi, J., Disordered, Sub-Nanometer Ru Structures on CeO_2 are Highly Efficient and Selective Catalysts in Polymer Upcycling by Hydrogenolysis. *ACS Catal.* **2022,** *12* (8), 4618-4627.
9. Chen, L.; Unocic, R. R.; Hoffman, A. S.; Hong, J.; Braga, A. H.; Bao, Z.; Bare, S. R.; Szanyi, J., Unlocking the Catalytic Potential of TiO_2-Supported Pt Single Atoms for the Reverse Water–Gas Shift Reaction by Altering Their Chemical Environment. *JACS Au* **2021,** *1* (7), 977-986.
10. Shao, X.; Prada, S.; Giordano, L.; Pacchioni, G.; Nilius, N.; Freund, H.-J., Tailoring the Shape of Metal Ad-Particles by Doping the Oxide Support. *Angew. Chem. Int. Ed.* **2011,** *50* (48), 11525-11527.
11. Risse, T.; Shaikhutdinov, S.; Nilius, N.; Sterrer, M.; Freund, H.-J., Gold Supported on Thin Oxide Films: From Single Atoms to Nanoparticles. *Acc. Chem. Res.* **2008,** *41* (8), 949-956.
12. Simic-Milosevic, V.; Heyde, M.; Lin, X.; König, T.; Rust, H.-P.; Sterrer, M.; Risse, T.; Nilius, N.; Freund, H.-J.; Giordano, L.; Pacchioni, G., Charge-Induced Formation of Linear Au Clusters on Thin MgO Films: Scanning Tunneling Microscopy and Density-Functional Theory Study. *Phys. Rev. B* **2008,** *78* (23), 235429.
13. Sterrer, M.; Risse, T.; Heyde, M.; Rust, H.-P.; Freund, H.-J., Crossover from Three-Dimensional to Two-Dimensional Geometries of Au Nanostructures on Thin MgO(001) Films: A Confirmation of Theoretical Predictions. *Phys. Rev. Lett.* **2007,** *98* (20), 206103.

14. Harding, C.; Habibpour, V.; Kunz, S.; Farnbacher, A. N.-S.; Heiz, U.; Yoon, B.; Landman, U., Control and Manipulation of Gold Nanocatalysis: Effects of Metal Oxide Support Thickness and Composition. *J. Am. Chem. Soc.* **2009,** *131* (2), 538-548.
15. Yoon, B.; Landman, U., Electric Field Control of Structure, Dimensionality, and Reactivity of Gold Nanoclusters on Metal-Supported MgO Films. *Phys. Rev. Lett.* **2008,** *100* (5), 056102.
16. Ricci, D.; Bongiorno, A.; Pacchioni, G.; Landman, U., Bonding Trends and Dimensionality Crossover of Gold Nanoclusters on Metal-Supported MgO Thin Films. *Phys. Rev. Lett.* **2006,** *97* (3), 036106.
17. Karim, A. M.; Prasad, V.; Mpourmpakis, G.; Lonergan, W. W.; Frenkel, A. I.; Chen, J. G.; Vlachos, D. G., Correlating Particle Size and Shape of Supported Ru/γ-Al_2O_3 Catalysts with NH_3 Decomposition Activity. *J. Am. Chem. Soc.* **2009,** *131* (34), 12230-12239.
18. Vaarkamp, M.; Modica, F. S.; Miller, J. T.; Koningsberger, D. C., Influence of Hydrogen Pretreatment on the Structure of the Metal-Support Interface in Pt/Zeolite Catalysts. *J. Catal.* **1993,** *144* (2), 611-626.
19. Koningsberger, D. C.; Gates, B. C., Nature of the Metal-Support Interface in Supported Metal Catalysts: Results from X-Ray Absorption Spectroscopy. *Catal. Letters* **1992,** *14* (3), 271-277.
20. Moller, K.; Koningsberger, D. C.; Bein, T., Stabilization of Metal Ensembles at Room Temperature: Palladium Clusters in Zeolites. *J. Phys. Chem. C* **1989,** *93* (16), 6116-6120.
21. Stakheev, A. Y.; Kustov, L. M., Effects of the Support on the Morphology and Electronic Properties of Supported Metal Clusters: Modern Concepts and Progress in 1990s. *Appl. Catal. A: Gen.* **1999,** *188* (1), 3-35.
22. Zhao, K.; Auerbach, D. J.; Campbell, C. T., Low-Energy Ion Scattering Intensities from Supported Nanoparticles: The Spherical Cap Model. *J. Phys. Chem. C* **2023,** *127* (19), 9129-9144.
23. Zhao, K.; Auerbach, D. J.; Campbell, C. T., Calorimetric Energies and Chemical Potentials of Metal Atoms in Catalytic Nanoparticles on Oxide and Carbon Supports: Improved Size Dependencies and Adhesion Energies. *ACS Catal.* **2023,** *13* (21), 13968-13981.
24. Mao, Z.; Rumptz, J. R.; Campbell, C. T., Energetics of Ag Adsorption on and Adhesion to Rutile TiO_2(100) Studied by Microcalorimetry. *J. Phys. Chem. C* **2021,** *125* (5), 3036-3046.
25. Hemmingson, S. L.; Campbell, C. T., Trends in Adhesion Energies of Metal Nanoparticles on Oxide Surfaces: Understanding Support Effects in Catalysis and Nanotechnology. *ACS Nano* **2017,** *11* (2), 1196-1203.
26. Campbell, C. T.; Mao, Z., Chemical Potential of Metal Atoms in Supported Nanoparticles: Dependence upon Particle Size and Support. *ACS Catal.* **2017,** *7* (12), 8460-8466.
27. Valero, M. C.; Raybaud, P.; Sautet, P., Nucleation of Pd_n (n=1-5) Clusters and Wetting of Pd Particles on γ-Al_2O_3 Surfaces: A Density Functional Theory Study. *Phys. Rev. B* **2007,** *75* (4), 045427.
28. Mammen, N.; Narasimhan, S., Inducing Wetting Morphologies and Increased Reactivities of Small Au Clusters on Doped Oxide Supports. *J. Chem. Phys.* **2018,** *149* (17), 174701.
29. Roberts, S.; Gorte, R. J., A Study of Platinum Films on Zirconia(100). *J. Phys. Chem.* **1991,** *95* (14), 5600-5604.
30. Alfredsson, M.; Richard, C.; Catlow, A., Predicting the Metal Growth Mode and Wetting of Noble Metals Supported on c-ZrO_2. *Surf. Sci.* **2004,** *561* (1), 43-56.
31. Stoneham, A. M., Systematics of Metal-Insulator Interfacial Energies: A New Rule for Wetting and Strong Catalyst-Support Interactions. *Appl. Surf. Sci.* **1983,** *14* (3), 249-259.

32. Thang, H. V.; Pacchioni, G.; DeRita, L.; Christopher, P., Nature of Stable Single Atom Pt Catalysts Dispersed on Anatase TiO_2. *J. Catal.* **2018,** *367*, 104-114.
33. Zandkarimi, B.; Poths, P.; Alexandrova, A. N., When Fluxionality Beats Size Selection: Acceleration of Ostwald Ripening of Sub-Nano Clusters. *Angew. Chem. Int. Ed.* **2021,** *60* (21), 11973-11982.
34. Kuo, C.-T.; Lu, Y.; Kovarik, L.; Engelhard, M.; Karim, A. M., Structure Sensitivity of Acetylene Semi-Hydrogenation on Pt Single Atoms and Subnanometer Clusters. *ACS Catal.* **2019**, 11030-11041.
35. Muravev, V.; Spezzati, G.; Su, Y.-Q.; Parastaev, A.; Chiang, F.-K.; Longo, A.; Escudero, C.; Kosinov, N.; Hensen, E. J. M., Interface Dynamics of Pd–CeO_2 Single-Atom Catalysts During CO Oxidation. *Nat. Catal.* **2021,** *4* (6), 469-478.
36. Daelman, N.; Capdevila-Cortada, M.; López, N., Dynamic Charge and Oxidation State of Pt/CeO_2 Single-Atom Catalysts. *Nat. Mater.* **2019,** *18* (11), 1215-1221.
37. Goodman, E. D.; Schwalbe, J. A.; Cargnello, M., Mechanistic Understanding and the Rational Design of Sinter-Resistant Heterogeneous Catalysts. *ACS Catal.* **2017,** *7* (10), 7156-7173.
38. Tang, Y.; Asokan, C.; Xu, M.; Graham, G. W.; Pan, X.; Christopher, P.; Li, J.; Sautet, P., Rh Single Atoms on TiO_2 Dynamically Respond to Reaction Conditions by Adapting Their Site. *Nat. Commun.* **2019,** *10* (1), 4488.
39. Chen, L.; Zhu, Y.; Meyer, L. C.; Hale, L. V.; Le, T. T.; Karkamkar, A.; Lercher, J. A.; Gutiérrez, O. Y.; Szanyi, J., Effect of Reaction Conditions on the Hydrogenolysis of Polypropylene and Polyethylene Into Gas and Liquid Alkanes. *React. Chem. Eng.* **2022,** *7* (4), 844-854.
40. Hackler, R. A.; Lamb, J. V.; Peczak, I. L.; Kennedy, R. M.; Kanbur, U.; LaPointe, A. M.; Poeppelmeier, K. R.; Sadow, A. D.; Delferro, M., Effect of Macro- and Microstructures on Catalytic Hydrogenolysis of Polyolefins. *Macromolecules* **2022,** *55* (15), 6801-6810.
41. Kots, P. A.; Xie, T.; Vance, B. C.; Quinn, C. M.; de Mello, M. D.; Boscoboinik, J. A.; Wang, C.; Kumar, P.; Stach, E. A.; Marinkovic, N. S.; Ma, L.; Ehrlich, S. N.; Vlachos, D. G., Electronic Modulation of Metal-Support Interactions Improves Polypropylene Hydrogenolysis Over Ruthenium Catalysts. *Nat. Commun.* **2022,** *13* (1), 5186.
42. Rorrer, J. E.; Troyano-Valls, C.; Beckham, G. T.; Román-Leshkov, Y., Hydrogenolysis of Polypropylene and Mixed Polyolefin Plastic Waste over Ru/C to Produce Liquid Alkanes. *ACS Sustainable Chem. Eng.* **2021,** *9* (35), 11661-11666.
43. Jentys, A., Estimation of Mean Size and Shape of Small Metal Particles by EXAFS. *Phys. Chem. Chem. Phys.* **1999,** *1* (17), 4059-4063.
44. NIST X-ray Photoelectron Spectroscopy Database, NIST Standard Reference Database Number 20, National Institute of Standards and Technology, Gaithersburg MD, 20899. (accessed 05/27).
45. Jablonski, A.; Powell, C. J., Relationships Between Electron Inelastic Mean Free Paths, Effective Attenuation Lengths, and Mean Escape Depths. *J. Electron Spectrosc. Relat. Phenom.* **1999,** *100* (1), 137-160.
46. Abdel-Mageed, A. M.; Wiese, K.; Hauble, A.; Bansmann, J.; Rabeah, J.; Parlinska-Wojtan, M.; Brückner, A.; Behm, R. J., Steering the Selectivity in CO_2 Reduction on Highly Active Ru/TiO_2 Catalysts: Support Particle Size Effects. *J. Catal.* **2021,** *401*, 160-173.
47. Li, Y.; Gao, Y., Interplay between Water and TiO_2 Anatase (101) Surface with Subsurface Oxygen Vacancy. *Phys. Rev. Lett.* **2014,** *112* (20), 206101.

48. Han, Y.; Liu, C.-j.; Ge, Q., Effect of Surface Oxygen Vacancy on Pt Cluster Adsorption and Growth on the Defective Anatase TiO_2(101) Surface. *J. Phys. Chem. C* **2007,** *111* (44), 16397-16404.
49. Murgida, G. E.; Ganduglia-Pirovano, M. V., Evidence for Subsurface Ordering of Oxygen Vacancies on the Reduced CeO_2(111) Surface Using Density-Functional and Statistical Calculations. *Phys. Rev. Lett.* **2013,** *110* (24), 246101.
50. Conesa, J. C., Computer Modeling of Surfaces and Defects on Cerium Dioxide. *Surf. Sci.* **1995,** *339* (3), 337-352.
51. ter Veen, H. R. J.; Kim, T.; Wachs, I. E.; Brongersma, H. H., Applications of High Sensitivity-Low Energy Ion Scattering (HS-LEIS) in heterogeneous catalysis. *Catal. Today* **2009,** *140* (3), 197-201.
52. Brongersma, H. H.; Jacobs, J.-P., Application of Low-Energy Ion Scattering to Studies of Growth. *Appl. Surf. Sci.* **1994,** *75* (1), 133-138.
53. Chambers, S. A.; Gao, Y.; Thevuthasan, S.; Liang, Y.; Shivaparan, N. R.; Smith, R. J., Molecular Beam Epitaxial Growth and Characterization of Mixed (Ti,Nb)O_2 Rutile Films on TiO_2(100). *J. Vac. Sci. Technol., A* **1996,** *14* (3), 1387-1394.
54. Jeziorowski, H.; Knözinger, H.; Taglauer, E.; Vogdt, C., Low Energy Ion Scattering Study of Ni-Mo-Al_2O_3 catalysts. *J. Catal.* **1983,** *80* (2), 286-295.
55. Bare, S. R.; Knop-Gericke, A.; Teschner, D.; Hävacker, M.; Blume, R.; Rocha, T.; Schlögl, R.; Chan, A. S. Y.; Blackwell, N.; Charochak, M. E.; ter Veen, R.; Brongersma, H. H., Surface analysis of zeolites: An XPS, variable kinetic energy XPS, and low energy ion scattering study. *Surf. Sci.* **2016,** *648*, 376-382.
56. Wasa, K., 2 - Sputtering Phenomena. In *Handbook of Sputtering Technology (Second Edition)*, Wasa, K.; Kanno, I.; Kotera, H., Eds. William Andrew Publishing: Oxford, 2012; pp 41-75.
57. Balajka, J.; Hines, M. A.; DeBenedetti, W. J. I.; Komora, M.; Pavelec, J.; Schmid, M.; Diebold, U., High-affinity Adsorption Leads to Molecularly Ordered Interfaces on TiO_2 in Air and Solution. *Science* **2018,** *361* (6404), 786-789.
58. Chen, L.; Kovarik, L.; Szanyi, J., Temperature-Dependent Communication between Pt/Al_2O_3 Catalysts and Anatase TiO_2 Dilutant: the Effects of Metal Migration and Carbon Transfer on the Reverse Water–Gas Shift Reaction. *ACS Catal.* **2021,** *11* (19), 12058-12067.
59. Coq, B.; Figueras, F., Structure–Activity Relationships in Catalysis by Metals: Some Aspects of Particle Size, Bimetallic and Supports Effects. *Coord. Chem. Rev.* **1998,** *178-180*, 1753-1783.
60. Bond, G. C.; Coq, B.; Dutartre, R.; Ruiz, J. G.; Hooper, A. D.; Proietti, M. G.; Sierra, M. C. S.; Slaa, J. C., Effect of Various Pretreatments on the Structure and Properties of Ruthenium Catalysts. *J. Catal.* **1996,** *161* (1), 480-494.
61. Coq, B.; Figueras, F., Influence of the Hydrocarbon Structure on the Hydrogenolysis of Alkanes Over Rhodium/Alumina Catalysts. *J. Mol. Catal.* **1987,** *40* (1), 93-112.
62. Flaherty, D. W.; Hibbitts, D. D.; Iglesia, E., Metal-Catalyzed C–C Bond Cleavage in Alkanes: Effects of Methyl Substitution on Transition-State Structures and Stability. *J. Am. Chem. Soc.* **2014,** *136* (27), 9664-9676.
63. Flaherty, D. W.; Iglesia, E., Transition-State Enthalpy and Entropy Effects on Reactivity and Selectivity in Hydrogenolysis of n-Alkanes. *J. Am. Chem. Soc.* **2013,** *135* (49), 18586-18599.

64. Tamura, M.; Miyaoka, S.; Nakaji, Y.; Tanji, M.; Kumagai, S.; Nakagawa, Y.; Yoshioka, T.; Tomishige, K., Structure-Activity Relationship in Hydrogenolysis of Polyolefins over Ru/Support Catalysts. *Appl. Catal. B: Environ.* **2022,** *318*, 121870.
65. Nakaji, Y.; Tamura, M.; Miyaoka, S.; Kumagai, S.; Tanji, M.; Nakagawa, Y.; Yoshioka, T.; Tomishige, K., Low-Temperature Catalytic Upgrading of Waste Polyolefinic Plastics Into Liquid Fuels and Waxes. *Appl. Catal. B: Environ.* **2021,** *285*, 119805.
66. Nakagawa, Y.; Oya, S.-i.; Kanno, D.; Nakaji, Y.; Tamura, M.; Tomishige, K., Regioselectivity and Reaction Mechanism of Ru-Catalyzed Hydrogenolysis of Squalane and Model Alkanes. *ChemSusChem* **2017,** *10* (1), 189-198.
67. Vance, B. C.; Kots, P. A.; Wang, C.; Granite, J. E.; Vlachos, D. G., Ni/SiO_2 Catalysts for Polyolefin Deconstruction via the Divergent Hydrogenolysis Mechanism. *Appl. Catal. B: Environ.* **2023,** *322*, 122138.
68. Chen, L.-N.; Wang, S.-H.; Zhang, P.-Y.; Chen, Z.-X.; Lin, X.; Yang, H.-J.; Sheng, T.; Lin, W.-F.; Tian, N.; Sun, S.-G.; Zhou, Z.-Y., Ru Nanoparticles Supported on Partially Reduced TiO_2 as Highly Efficient Catalyst for Hydrogen Evolution. *Nano Energy* **2021,** *88*, 106211.
69. Cline, D., *Variational Principles in Classical Mechanics*. University of Rochester River Campus Librarie: 2017.
70. Zandkarimi, B.; Poths, P.; Alexandrova, A. N., When Fluxionality Beats Size Selection: Acceleration of Ostwald Ripening of Sub-Nano Clusters. *Angew. Chem. Int. Ed.* **2021,** *60* (21), 11973-11982.
71. Zhai, H.; Alexandrova, A. N., Fluxionality of Catalytic Clusters: When It Matters and How to Address It. *ACS Catal.* **2017,** *7* (3), 1905-1911.
72. Alexandrova, A. N.; Boldyrev, A. I., σ-Aromaticity and σ-Antiaromaticity in Alkali Metal and Alkaline Earth Metal Small Clusters. *J. Phys. Chem. A* **2003,** *107* (4), 554-560.
73. H.-Y. T. Chen; Tosoni, S.; Pacchioni, G., Hydrogen Adsorption, Dissociation, and Spillover on Ru_{10} Clusters Supported on Anatase TiO_2 and Tetragonal ZrO_2 (101) Surfaces. *ACS Catal.* **2015,** *5*, 5486–5495.
74. Mager-Maury, C.; Bonnard, G.; Chizallet, C.; Sautet, P.; Raybaud, P., H_2-Induced Reconstruction of Supported Pt Clusters: Metal–Support Interaction versus Surface Hydride. *ChemCatChem* **2010,** *3*, 200-207.
75. A. Gorczyca; V. Moizan; C. Chizallet; O. Proux; W. D. Net; E. Lahera; J.-L. Hazemann; P. Raybaud; Joly, Y., Monitoring Morphology and Hydrogen Coverage of Nanometric Pt/γ-Al_2O_3 Particles by In Situ HERFD–XANES and Quantum Simulations. *Angew. Chem. Int. Ed.* **2014,** *53*, 12426-12429.
76. X.-P. Wu; Gong, X.-Q.; Lu, G., Role of Oxygen Vacancies in the Surface Evolution of H at CeO_2(111): A Charge Modification Effect. *Phys. Chem. Chem. Phys. 17*, 3544-3549.
77. P. Liu; C. Zheng; W. Liu; X. Wu; Liu, S., Oxidative Redispersion-Derived Single-Site Ru/CeO_2 Catalysts with Mobile Ru Complexes Trapped by Surface Hydroxyls Instead of Oxygen Vacancies. *ACS Catal.* **2024,** *14*, 6028–6044.
78. Lemire, C.; Meyer, R.; Shaikhutdinov, S. K.; Freund, H. J., CO Adsorption on Oxide Supported Gold: from Small Clusters to Monolayer Islands and Three-Dimensional Nanoparticles. *Surf. Sci.* **2004,** *552* (1), 27-34.
79. Freund, H.-J., Clusters and Islands on Oxides: From Catalysis via Electronics and Magnetism to Optics. *Surf. Sci.* **2002,** *500* (1), 271-299.
80. Böttcher, A.; Niehus, H., Oxygen Adsorbed on Oxidized Ru(0001). *Phys. Rev. B* **1999,** *60* (20), 14396.

81. Skriver, H. L.; Rosengaard, N. M., Surface Energy and Work Function of Elemental Metals. *Phys. Rev. B* **1992,** *46* (11), 7157-7168.
82. Derry, G. N.; Kern, M. E.; Worth, E. H., Recommended Values of Clean Metal Surface Work Functions. *J. Vac. Sci. Technol., A.* **2015,** *33* (6), 060801.
83. Xue, C.; An, H.; Shao, G.; Yang, G., Accelerating Directional Charge Separation via Built-in Interfacial Electric Fields Originating from Work-Function Differences. *Chin. J. Catal.* **2021,** *42* (4), 583-594.
84. Mansfeldova, V.; Zlamalova, M.; Tarabkova, H.; Janda, P.; Vorokhta, M.; Piliai, L.; Kavan, L., Work Function of TiO_2 (Anatase, Rutile, and Brookite) Single Crystals: Effects of the Environment. *J. Phys. Chem. C* **2021,** *125* (3), 1902-1912.
85. Das, D.; Shyam, S., Reduced Work Function in Anatase ⟨101⟩ TiO_2 Films Self-Doped by O-Vacancy-Dependent Ti^{3+} Bonds Controlling the Photocatalytic Dye Degradation Performance. *Langmuir* **2024,** *40* (20), 10502-10517.
86. Wardenga, H. F.; Klein, A., Surface Potentials of (111), (110) and (100) Oriented CeO_{2-x} Thin Films. *Appl. Surf. Sci.* **2016,** *377*, 1-8.
87. Herman, G. S., Characterization of surface defects on epitaxial CeO_2(001) films. *Surf. Sci.* **1999,** *437* (1), 207-214.
88. Chen, H. T.; Chang, J. G.; Chen, H. L.; Ju, S. P., Identifying the O_2 Diffusion and Reduction Mechanisms on CeO_2 Electrolyte in Solid Oxide Fuel Cells: A DFT + U Study. *J. Comput. Chem* **2009,** *30* (15), 2433-42.
89. Chen, H.-Y. T.; Tosoni, S.; Pacchioni, G., Adsorption of Ruthenium Atoms and Clusters on Anatase TiO_2 and Tetragonal ZrO_2 (101) Surfaces: A Comparative DFT Study. *J. Phys. Chem. C* **2015,** *119* (20), 10856-10868.
90. Rahman, M. S.; Paudyal, N.; Hill, L. D.; Zhou, J.; Xu, Y., The Structure, Oxidation States, and Energetics of Co Nanoparticles on CeO_2(111): An STM and DFT Study. *J. Phys. Chem. C* **2024,** *128*, 18430-18441.
91. Khivantsev, K.; Pham, H.; Engelhard, M. H.; Aleksandrov, H. A.; Kovarik, L.; Bowden, M.; Li, X. S.; Tian, J.; Koleva, I. Z.; Song, I.; Hu, W.; Wei, X.; Sun, Y.; Tran, P.; Graham, T. R.; Jiang, D.; Dean, D. P.; Breckner, C. J.; Miller, J. T.; Vayssilov, G. N.; Szanyi, J.; Datye, A.; Wang, Y., Transforming Ceria into 2D Clusters Enhances Catalytic Activity. *Nature* **2025,** *640* (8060), 947-953.

TOC Graphic

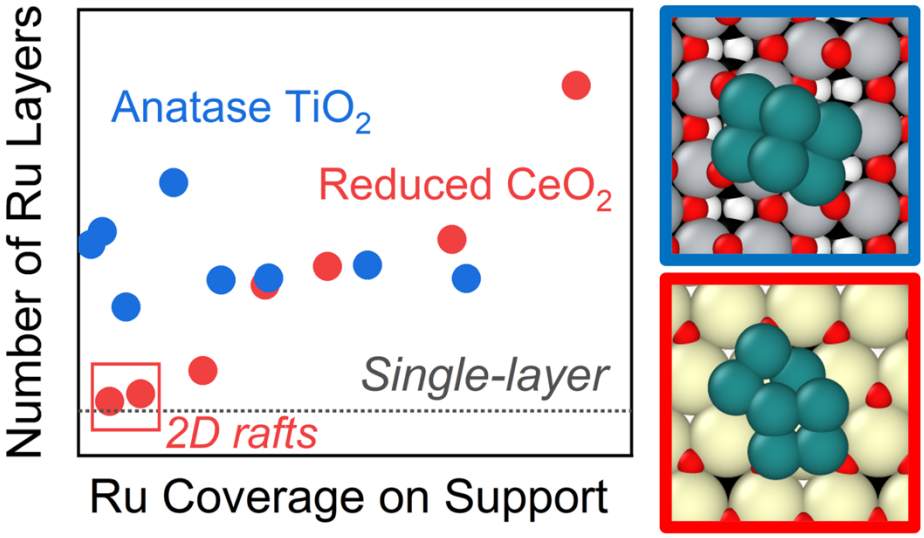
Number of Ru Layers
Anatase TiO_2
Reduced CeO_2
Single-layer
2D rafts
Ru Coverage on Support